ACS APPLIED MATERIALS & INTERFACES

www.acsami.org

Research Article

Design of a High-Performance Titanium Nitride Metastructure-Based Solar Absorber Using Quantum Computing-Assisted Optimization

Seongmin Kim, Shiwen Wu, Ruda Jian, Guoping Xiong,* and Tengfei Luo*

Cite This: *ACS Appl. Mater. Interfaces* 2023, 15, 40606−40613

Read Online

ACCESS | Metrics & More | Article Recommendations | Supporting Information

ABSTRACT: Metastructures of titanium nitride (TiN), a plasmonic refractory material, can potentially achieve high solar absorptance while operating at elevated temperatures, but the design has been driven by expert intuition. Here, we design a high-performance solar absorber based on TiN metastructures using quantum computing-assisted optimization. The optimization scheme includes machine learning, quantum annealing, and optical simulation in an iterative cycle. It designs an optimal structure with solar absorptance > 95% within 40 h, much faster than an exhaustive search. Analysis of electric field distributions demonstrates that combined effects of Fabry−Perot interferences and surface plasmonic resonances contribute to the broadband high absorption efficiency of the optimally designed metastructure. The designed absorber may exhibit great potential for solar energy harvesting applications, and the optimization scheme can be applied to the design of other complex functional materials.

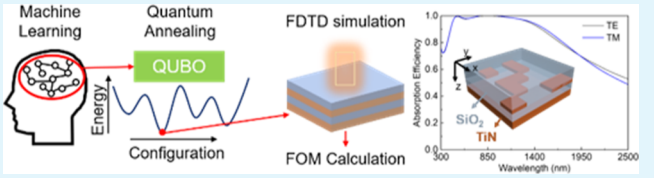

KEYWORDS: *metastructure, solar absorber, thermophotovoltaic, quantum computing, machine learning*

1. INTRODUCTION

Solar energy is the most abundant, clean, and sustainable resource for addressing global energy and environmental challenges.[1−3] Therefore, solar energy harvesting has attracted great attention over the past few decades for converting solar energy into electricity for human use.[4−6] Among these applications, thermophotovoltaic (TPV) systems can be one of the most efficient technologies as the theoretical efficiency of TPVs (∼85.4%) is much higher than the Shockley−Queisser efficiency.[7−14] TPV systems generally include an absorber, an emitter, and a photovoltaic (PV) cell, where solar energy should be efficiently absorbed by the absorber (ideally 100%) in the solar spectrum range ($300 < \lambda < 2500$ nm).[15,16] Noble materials that show plasmonic effects in the solar spectrum, such as gold and silver, can be candidates for the absorber, but they cannot be used for TPV systems because of their weak chemical or thermal stabilities at elevated temperatures (>1300 K).[17−19] Despite their high absorption efficiency, carbon-based materials also cannot be used for the TPV absorber due to the usual high working temperature of TPV systems.[20] Therefore, refractory materials that can withstand high working temperatures should be used (*e.g.*, titanium nitride (TiN), tungsten, or tantalum carbide).[21,22] TiN-based materials have been extensively studied for TPV systems because they can show plasmonic effects in the solar spectrum and excellent stability and durability at high temperatures (the melting temperature of TiN is ∼3200 K).[23,24] However, designing a simple TiN layer to achieve high absorption efficiency over the entire solar spectrum is rather difficult due to its metallic properties, especially in the wavelength range of $\lambda > 550$ nm.[25] In the past decade, there have been attempts to design solar absorbers using TiN-based structures for high solar absorptance, such as TiN-based metamaterials,[25−27] and TiN-based metal−insulator−metal absorbers.[28] Among them, some TiN metastructure-based absorbers could achieve a high solar absorptance of up to 94%,[26,27] but there should still be room for improvement. However, it is challenging to find the optimal design of metastructure absorbers due to the large design space.

In the recent decade, optimization approaches leveraging machine learning have emerged as efficient tools for the inverse design of complex materials such as metastructures.[29−32] The optimization could successfully design various photonic structures to achieve high performance.[33,34] However, designing discretized structures, such as those seen in metastructures, can be difficult for conventional gradient-based schemes to find the global optimum due to the lack of gradient. In discrete optimization spaces, the only approach that guarantees the finding of the global optimum is an exhaustive search, but when the degree of freedom is large, it becomes insurmount-

Received: June 7, 2023
Accepted: August 8, 2023
Published: August 18, 2023

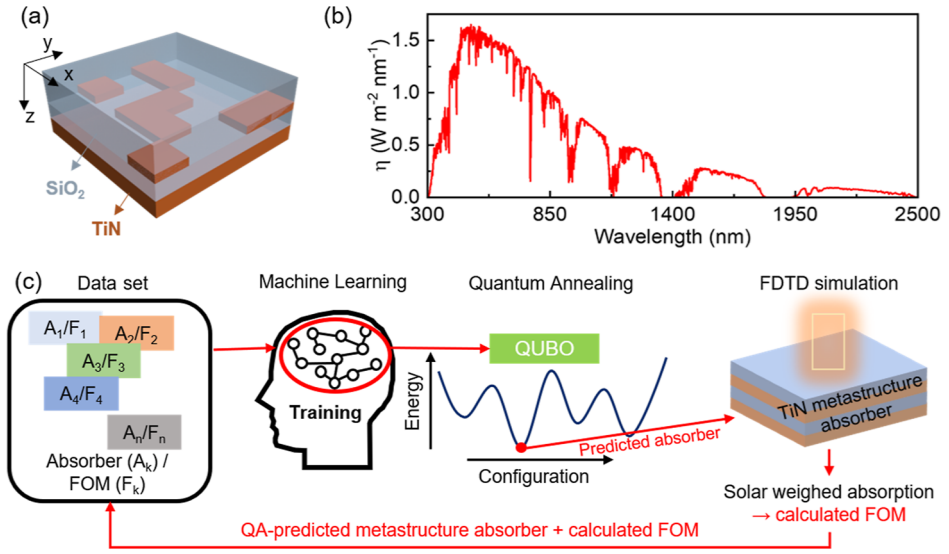

Figure 1. (a) Schematic of a TiN metastructure-based absorber consisting of an upper SiO_2 layer, a TiN pattern layer in the middle, and a lower SiO_2 layer on a TiN substrate. (b) Solar-weighted absorption (η) of an ideal absorber. (c) Schematic of the QA-assisted optimization process, including data generation, machine learning, QA optimization, and FDTD simulation in an iterative loop.

able for classical computers to exhaustively enumerate all possible candidates. To overcome these limitations, quantum computing-assisted optimization schemes have been proposed recently.[35−37] In the schemes, a machine learning surrogate model is used to describe the relationship between the inputs and the target property, and quantum annealing (QA), a quantum computing scheme, efficiently predicts the best structure based on the surrogate model. QA can quickly evaluate a large number of possible combinations of input parameters via quantum superposition to find the lowest energy state in the optimization space, and it will not be stuck in local minima thanks to the quantum tunneling effect.[35,37] When dealing with small-scale problems, despite its faster convergence, QA-assisted optimization strategies may not provide a significant advantage over classical methods, which can be a more cost-effective choice. Hence, it is essential to carefully choose between classical and quantum computing schemes for solving small-scale problems, considering the associated costs. However, for large-scale optimization that classical methods cannot handle, QA-assisted optimization strategies are efficient solutions to solve optimization problems, providing exceptional capabilities in large optimization spaces.

In this paper, we design a TiN metastructure for high solar absorptance using the QA-assisted optimization scheme. TiN pattern configurations, TiN layer thickness, and dielectric layer thicknesses are optimized. The optimally designed absorber shows a high solar absorptance (>95% of total solar energy), which is attributed to the high absorption efficiency of the absorber especially in the visible/near-infrared regions where solar irradiance is intense (average absorption efficiency is >98% in $400 < \lambda < 1300$ nm). We perform electromagnetic wave calculations to show that the high absorption originates from the combined effect of Fabry−Perot interferences and localized surface plasmon resonances. We expect that the proposed TiN metastructure absorber can be broadly used for TPV applications. Furthermore, the optimization process demonstrates the high efficiency of the QA-assisted optimization scheme to design complex metastructures.

2. DESIGN OF A TIN METASTRUCTURE-BASED SOLAR ABSORBER

Figure 1a shows the schematic diagram of a TiN metastructure-based absorber that consists of an upper silicon dioxide (SiO_2) layer, a TiN pattern layer, and a lower SiO_2 layer on a 150 nm-thick TiN substrate with a unit cell size of 500 nm × 500 nm. We aim to optimize the TiN pattern configurations and geometric parameters, including the upper SiO_2 layer thickness (d_1), the TiN pattern layer thickness (d_2), and the lower SiO_2 layer thickness (d_3), to achieve high solar absorptance (see Figure S1). The TiN pattern layer is divided into $n \times n$ pixels, and thus, the side of each square pixel is 500/n nm. Each pixel can be either SiO_2 or TiN, where SiO_2 is denoted as "0" and TiN is denoted as "1" to express pattern configurations as binary vectors. The whole structure can be regarded as TiN patterns embedded in a SiO_2 medium. We set eight candidate values for d_1: 0, 20, 40, 60, 80, 100, 120, and 140 nm, with them denoted as binary labels of "000", "001", "010", "011", "100", "101", "110", and "111", respectively. There are four candidate values for d_2: 10, 15, 20, and 25 nm, which are denoted as binary labels of "00", "01", "10", and "11", respectively. Another eight candidate values are used for d_3: 60, 70, 80, 90, 100, 110, 120, and 130 nm, which are denoted as binary labels of "000", "001", "010", "011", "100", "101", "110", and "111", respectively. Hence, any TiN metastructure-based absorber with a TiN pattern configuration and any of the above layer thicknesses can be expressed as a binary vector. For example, an absorber with a TiN pattern configuration [see Figure S1(a), 4 × 4 pixels], an upper SiO_2 layer thickness (d_1) of 60 nm, a TiN pattern layer thickness (d_2) of 20 nm, and a lower SiO_2 layer thickness (d_3) of 80 nm can be represented by a binary vector of [010010010110101001110010]. Our objective is to design TiN metastructure absorbers with solar absorptance approaching that of an ideal solar absorber (*i.e.*, 100% of absorption efficiency in the solar spectrum, see Figure 1b). We achieve this objective by optimizing the pattern configuration and layer thicknesses using the QA-assisted optimization scheme.

https://doi.org/10.1021/acsami.3c08214
ACS Appl. Mater. Interfaces 2023, 15, 40606−40613

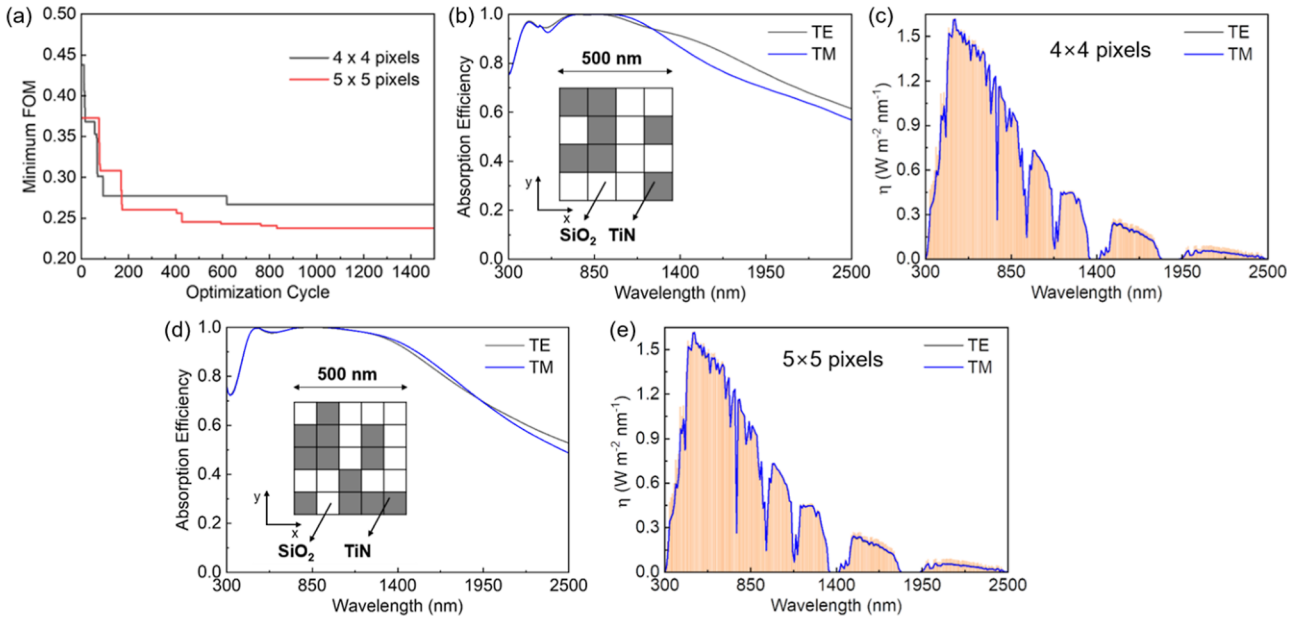

Figure 2. (a) Optimization results of the design of TiN metastructure absorbers (4 × 4 and 5 × 5 pixels). (b,d) Absorption efficiency of the optimal absorber (4 × 4 and 5 × 5 pixels) in the solar spectrum for the TE and TM polarizations. Insets: the optimal TiN patterns. The binary vector of the optimal absorber (4 × 4 pixels) is [0101011100001010010011001]; in this absorber, d_1 is 80 nm, d_2 is 25 nm, and d_3 is 70 nm. The binary vector of the optimal absorber (5 × 5 pixels) is [1011000111110001011010000010111001]; d_1 is 100 nm, d_2 is 25 nm, and d_3 is 70 nm. (c,e) Solar-weighted absorption of the optimal absorber (4 × 4 and 5 × 5 pixels) for the TE and TM polarizations. Notably, the two lines almost overlap. Orange shade indicates solar-weighted absorption of the ideal absorber.

3. SIMULATION AND OPTIMIZATION

We use the finite difference time domain (FDTD) method (Lumerical 2022, Ansys) to calculate the optical characteristics of the TiN metastructure-based absorbers. For the simulation, we employ periodic boundary conditions in the x and y directions, and perfectly matched layers in the z direction as the absorbing boundary.[27] The optical properties of the SiO_2 and TiN are from the literature.[38] In addition, we set a plane wave incident to the upper SiO_2 layer along the z direction (see Figure 1c, FDTD simulation). Transverse electric (TE) polarization is denoted when the polarization is along the x-axis (polarization angle = 0° in the simulation), and transverse magnetic (TM) polarization is denoted when the polarization is along with the y-axis (polarization angle = 90° in the simulation), as shown in the schematic in Figure S1c. Absorption efficiency can be calculated from $A(\lambda) = 1 - T(\lambda) - R(\lambda)$, where $T(\lambda)$ and $R(\lambda)$ represent transmission and reflection efficiency, respectively.[39] Based on the calculated absorption efficiency, solar-weighted absorption is calculated from $\eta(\lambda) = A(\lambda) \times S(\lambda)$, where $S(\lambda)$ is the solar spectral irradiance. To define the performance of the designed TiN metastructure absorber, a figure-of-merit (FOM) is calculated by

$$\mathrm{FOM}_{\mathrm{TE\ or\ TM}} = \frac{5 \times \int (\eta_{\mathrm{ideal}}(\lambda) - \eta_{\mathrm{designed,TE\ or\ TM}}(\lambda))\, \mathrm{d}\lambda}{\int S(\lambda)\, \mathrm{d}\lambda} \tag{1}$$

where $\eta_{\mathrm{ideal}}(\lambda)$ is the solar-weighted absorption of an ideal absorber, and $\eta_{\mathrm{designed,TEorTM}}(\lambda)$ is the solar-weighted absorption of the designed absorber in the solar spectrum under the TE- or TM-polarized light. Polarization insensitivity is important for practical applications of solar absorbers,[40,41] and the final FOM is thus an average of $\mathrm{FOM}_{\mathrm{TE}}$ and $\mathrm{FOM}_{\mathrm{TM}}$. The FOM essentially measures how close a designed absorber is to the ideal absorber. Therefore, a lower FOM means that an absorber has better solar energy-absorbing performance in the solar spectrum. The solar absorptance of an absorber (α) is calculated by

$$\alpha = \frac{\int \eta(\lambda)\, \mathrm{d}\lambda}{\int S(\lambda)\, \mathrm{d}\lambda} \tag{2}$$

For the optimization, we use binary vectors (representing absorbers with different TiN pattern configurations and different layer thicknesses) and their corresponding FOMs as data sets. The optimization process is as follows: (1) Preparing an initial data set by generating 25 random metastructure absorbers and calculating their FOMs, (2) training a factorization machine (FM) model as the machine learning surrogate with the initial data set, (3) constructing a quadratic unconstrained binary optimization (QUBO) matrix based on the trained FM model parameters and finding the binary vector that gives the lowest energy state of the QUBO objective function using QA, (4) conducting FDTD simulation of the predicted metastructure absorber from step (3) and calculating its FOM, and (5) updating the training data set by adding the new metastructure (in a binary vector) and the calculated FOM. The optimal structure can be identified by iterating these steps until convergence is reached (see Figure 1c). We note that one can vary the size of the initial training data set, but no apparent speed-up in convergence is observed when the data set size is greater than 25. Additionally, in step (3), the QA-identified optimal binary vector may already exist in the data set. To provide more diversity in the training data set, in this case, we choose a random binary vector instead of the repeated binary vector in steps (4) and (5).

https://doi.org/10.1021/acsami.3c08214
ACS Appl. Mater. Interfaces 2023, 15, 40606−40613

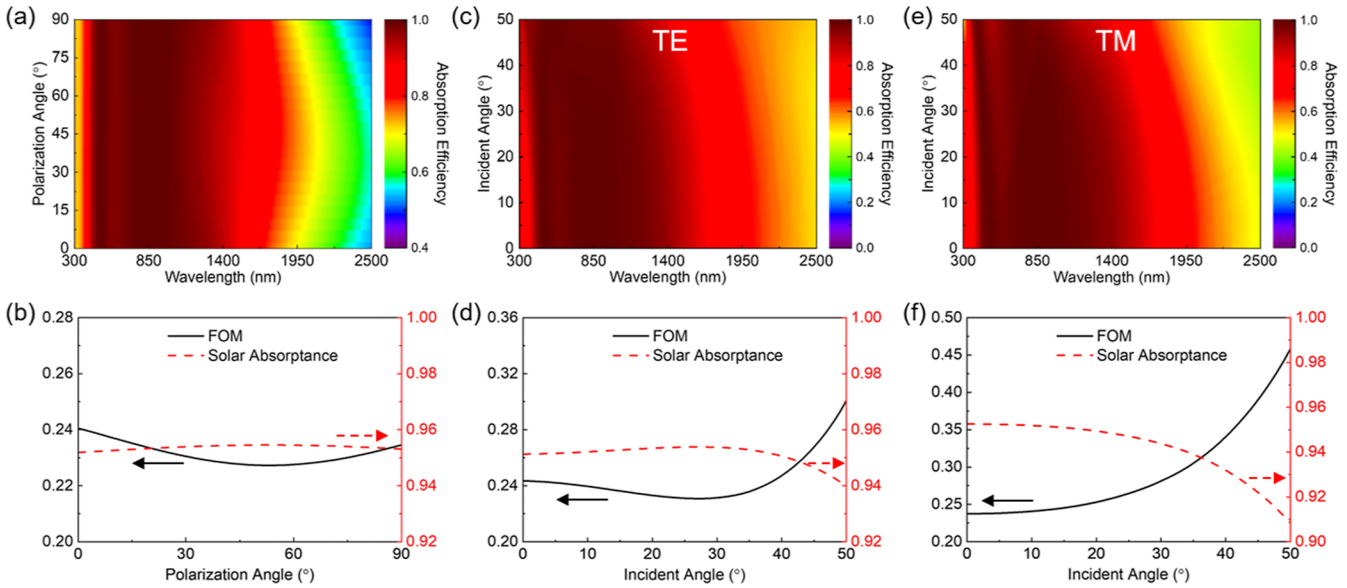

Figure 3. (a) Absorption efficiency in the solar spectrum and (b) FOM and solar absorptance of the optimal absorber (5 × 5 pixels) with different polarization angles under normal incident light. (c,e) Absorption efficiency in the solar spectrum and (d,f) FOM and solar absorptance of the optimal absorber with different incident angles for the TE polarization and TM polarization, respectively.

4. RESULTS AND DISCUSSION

We have studied metastructure absorbers consisting of 4 × 4 pixels and 5 × 5 pixels of the TiN pattern layer. For the structure with 4 × 4 pixels and different layer thicknesses, the binary vector length is 24, which corresponds to a design space of 2^{24}. It becomes 2^{33} when the pattern layer has 5 × 5 pixels. Exhaustive enumeration of all structures using FDTD to find the global optimal structure is impossible since it will take more than 40 and 20,000 years for metastructure absorbers with 4 × 4 and 5 × 5 pixels pattern layers, respectively. In contrast, our QA-assisted optimization can find the optimal structures within 40 h. Figure 2a shows the minimum FOM as a function of optimization cycles, showing that convergence is reached with 1500 cycles. Figure 2b shows the absorption efficiencies of the absorber with the optimal TiN pattern (4 × 4 pixels, each pixel size is 125 × 125 nm) and the optimal layer thicknesses. This absorber has a low FOM of 0.2666. It should be noted that the FOM definition we set gives higher priority to the region where solar irradiance is intense. Hence, the absorber has a high absorption efficiency with an average value of over 97% in the wavelength range ($400 < \lambda < 1300$ nm) where solar irradiance is high. The absorption efficiency is low in the region $\lambda > 1300$ nm, but solar-weighted absorption is still high, close to the ideal absorber. Therefore, in the whole solar spectrum range, the solar-weighted absorption is very high, resulting in a low FOM (see Figure 2c). It is worth noting that the optimal TiN metastructure absorber shows polarization insensitivity although this absorber is not symmetric in the $x-y$ plane, unlike previously reported polarization-independent solar absorbers achieved by strict geometric symmetry.[25,42,43] This means that our optimization scheme can find the optimal absorber considering both TE and TM polarizations, which is attributed to the FOM definition including both polarizations. Hence, the optimally designed absorber shows low FOMs for both TE and TM polarizations (FOM_{TE} = 0.2433 and FOM_{TM} = 0.2899). In addition, the solar-weighted absorption of the optimal absorber is close to that of the ideal absorber, showing a high solar absorptance of 94.67% (95.13% for the TE polarization and 94.2% for the TM polarization) (see Figure 2c). With the finer pixel size of 100 nm × 100 nm (5 × 5 pixels) for the TiN pattern, a better absorber can be achieved with a lower FOM of 0.2375 (FOM_{TE} = 0.2405 and FOM_{TM} = 0.2345). This absorber also has high absorption efficiency with an average value of over 98% in the wavelength range ($400 < \lambda < 1300$ nm) (see Figure 2d). The solar absorptance of the absorber is 95.25%, and it is also insensitive to polarizations (95.19% for the TE polarization and 95.31% for the TM polarization), which is closer to that of the ideal absorber, as shown in Figure 2e.

Insensitivity to the polarization angle and incident angle of the designed absorber is important for real-world applications as mentioned above. Since our TiN metastructure-based absorbers are not rotationally symmetric, absorbers with a low FOM for the TE polarization may not simultaneously have a low FOM for the TM polarization. For instance, we first design absorbers considering only the TE polarization. In this case, FOM_{TE} is used but FOM_{TM} is not used during optimization, so the FOM is the same as the FOM_{TE}. The optimal absorber has a low FOM of 0.1943 and high absorption efficiency (96.11%) in the solar spectrum when the polarization angle is 0° (TE polarization) since the absorber is optimized under this condition. However, the absorption performance deteriorates with the increasing polarization angle (see Figure S3a). Consequently, the absorber has a high FOM of 0.6631 when the polarization angle is 90° (TM polarization), corresponding to a solar absorptance of 86.74% (see Figure S3b). This absorber is not suitable for solar energy harvesting applications as it inevitably has poor solar absorptance due to randomly polarized sunlight. When both TE and TM polarizations are considered in the FOM, *i.e.*, $FOM = (FOM_{TE} + FOM_{TM})/2$, the optimal design has a much better solar absorptance. Figure 3a presents the absorption efficiency of the optimal absorber (5 × 5 pixels) with different polarization angles from 0° (TE polarization) to 90° (TM polarization) under normal incident light. It should be noted that high absorption efficiency is preserved even with

https://doi.org/10.1021/acsami.3c08214
ACS Appl. Mater. Interfaces 2023, 15, 40606−40613

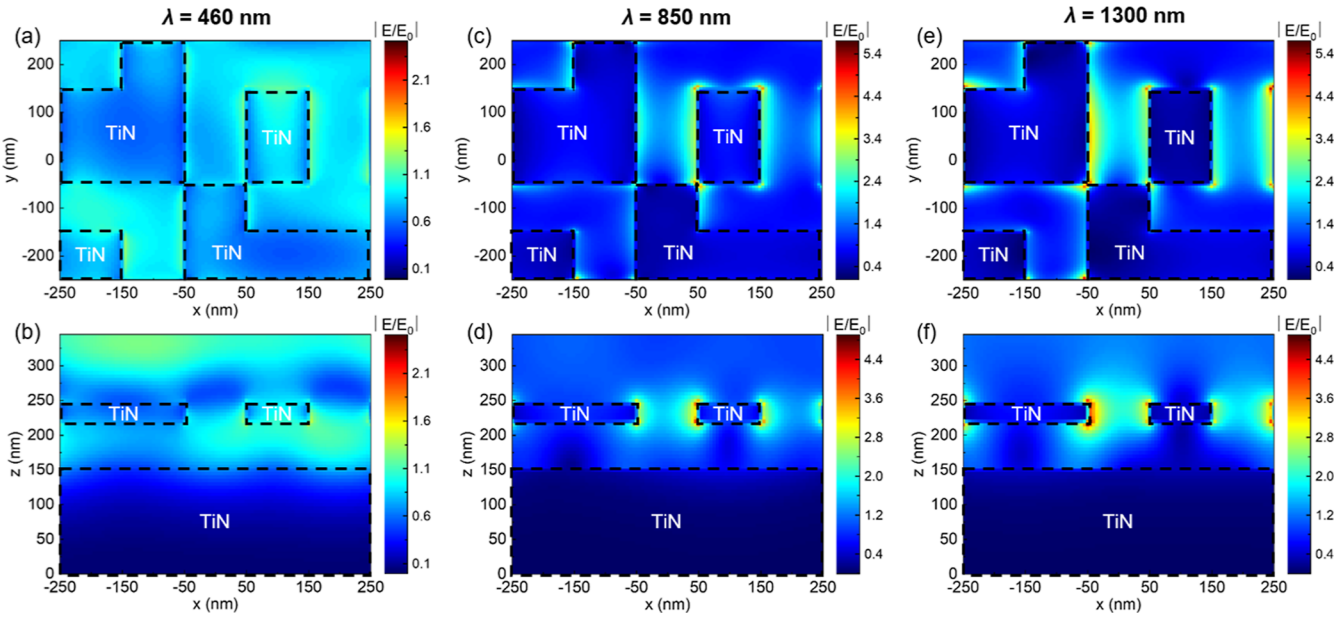

Figure 4. Electric field distribution in the optimal TiN metastructure absorber with normal incident light (TE polarization) at λ = (a,b) 460 nm, (c,d) 850 nm, and (e,f) 1300 nm. (a,c,e) shows the electric field distribution in the $x-y$ plane at the TiN pattern layer (at z = 232.5 nm). (b,d,f) shows the electric field distribution in the $x-z$ plane (at y = 50 nm).

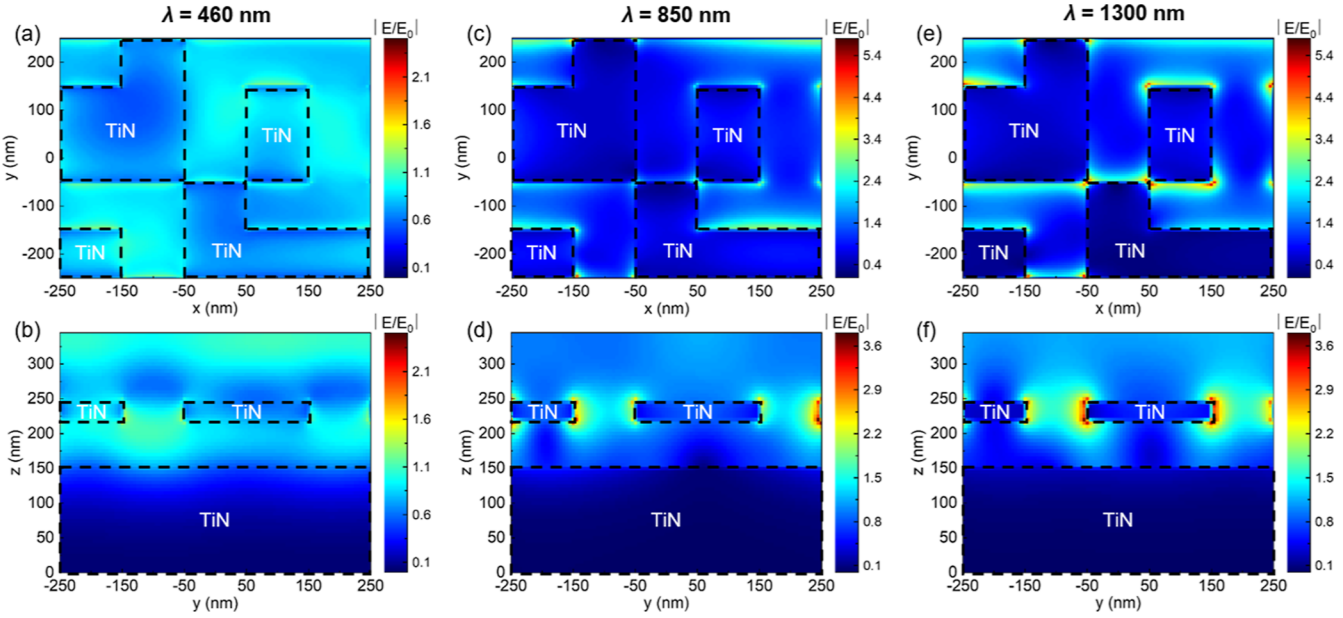

Figure 5. Electric field distribution in the optimal TiN metastructure absorber with normal incident light (TM polarization) at λ = (a,b) 460 nm, (c,d) 850 nm, and (e,f) 1300 nm. (a,c,e) shows the electric field distribution in the $x-y$ plane at the TiN pattern layer (at z = 232.5 nm). (b,d,f) shows the electric field distribution in the $y-z$ plane (at x = −200 nm).

an increasing polarization angle, which leads to consistently low FOM values (from 0.2273 at the polarization angle of 52° to 0.2405 at the polarization angle of 0°) in all polarization angles (see Figure 3b). Therefore, solar absorptance is high in all polarization angles (from 95.19% at 0° to 95.45% at 52°). Moreover, the absorber exhibits high solar absorptance within a wide range of incident angles. Figure 3c,e shows the absorption efficiency of the absorber with different incident angles from 0 to 50° for the TE and TM polarization, respectively. The FOM at any incident angle is always lower than 0.4581, which means solar absorptance at any incident angle is always higher than 90.84% (see Figure 3d,f). These results demonstrate the polarization and incident angle insensitivity of the absorber, although the TiN metastructure is not rotationally invariant. As a result, these optical characteristics along with the refractory properties of the used materials make the absorber more suitable for high-temperature solar energy harvesting applications such as TPV.

Electric field distributions within the optimal TiN absorber at the different wavelengths (λ = 460, 850, and 1300 nm) are calculated to analyze the origin of such high absorption efficiency in the solar spectrum. Figure 4 shows electric field distributions in the $x-y$ and $x-z$ planes under normally incident TE-polarized light. Figure 4a,b presents the electric

https://doi.org/10.1021/acsami.3c08214
ACS Appl. Mater. Interfaces 2023, 15, 40606−40613

field distribution in the absorber at λ = 460 nm. No strong electric field localization is observed in the TiN pattern layer, indicating that TiN behaves as a lossy dielectric at short wavelengths. In the $x-z$ plane shown in Figure 4b, the electric field in the top SiO_2 layer is intense, indicating that the top dielectric layer acts as an anti-reflective layer and contributes to the nearly perfect absorption around λ = 460 nm. In addition, a strong electric field can be observed in the SiO_2 layer sandwiched between two TiN layers. This can be attributed to the Fabry−Perot resonance induced by the two mirror-like TiN layers and the sandwiched SiO_2 layer,[27,44] which is consistent with the features of Fabry−Perot cavities observed in our prior work.[26,27] At λ = 850 nm, strong electric field enhancements are observed at the edges of TiN patterns in the $x-y$ and $x-z$ planes (see Figure 4c,d). Such a strongly localized electric field can be attributed to plasmon hybridization between the adjacent TiN patterns,[27,44,45] which leads to nearly perfect absorption (absorption efficiency = 99.98%) at this wavelength. This conclusion can be further verified by the distributions of the vertical component of electric fields (E_z) in the $x-z$ plane (see Figure S4a), where apparent dipoles can be observed along the edges of TiN patterns. Similarly, at λ = 1300 nm where the absorption efficiency is high (96.04%), the electric field is also primarily distributed at the edges of the TiN patterns (see Figure 4e,f). Moreover, the dipoles observed in the E_z distribution at λ = 1300 nm exhibit opposite polarities to the ones at λ = 850 nm (Figure S4), illustrating that the strong absorption at these two wavelengths is caused by antisymmetric and symmetric plasmon hybridization between two adjacent TiN edges.[46,47]

The optimally designed absorber shows polarization insensitivity despite the non-symmetric geometry of the TiN metastructure, with a high solar absorptance of 95.31% achieved under the TM-polarized light. We further investigate the electric field distribution in the $x-y$ and $y-z$ planes under normally incident TM-polarized light, as shown in Figure 5. Similar to the electric field distributions under the TE-polarized light, Fabry−Perot resonance and the top anti-reflective SiO_2 layer contribute to the high absorption (98.55%) at λ = 460 nm (see Figure 5a,b). In addition, high absorption efficiencies at λ = 850 and 1300 nm (99.93 and 96.47%, respectively) are caused by plasmon hybridization between adjacent TiN patterns, which can be verified by the significantly enhanced electric field at the edges and the apparent dipoles observed in the E_z distributions (see Figures 5c,f, and S5). In short, benefiting from the extended light absorption range due to the combined effects of Fabry−Perot resonances and plasmon hybridization between adjacent TiN patterns, the optimal TiN metastructure absorber exhibits high absorption performance in both TE and TM polarizations across the whole solar spectrum, especially in the range where the solar irradiance is high ($400 < \lambda < 1300$ nm). This TiN metastructure absorber can be fabricated by the nano-patterning technique using e-beam lithography.[48] TiN and SiO_2 layers can be prepared using plasma-enhanced chemical vapor deposition, pulsed laser deposition, or physical vapor deposition.[49,50] While TiN and SiO_2 deposition can be inexpensive, the lithography process for the metastructure may incur higher expenses. Despite the initial fabrication costs, the outstanding stability of those materials may ensure long-term usage of the fabricated solar absorber, making it promising for real-world applications.[23,51] These fabrication processes will be conducted for experimental characterization and demonstration in future work.

5. CONCLUSIONS

In this work, using a QA-assisted optimization scheme, we have designed a high-performance TiN metastructure solar absorber, which consists of a SiO_2 layer on the top, a TiN pattern layer in the middle, and a SiO_2 layer at the bottom on a TiN substrate. The optimal configuration for the TiN pattern and optimal thicknesses for the SiO_2 and pattern layer are identified by QA optimization. The optimally designed absorber has a high absorption efficiency (>98%) in the visible/near-infrared wavelength range ($400 < \lambda < 1300$ nm) where solar irradiance is high, which results in a high solar absorptance (over 95%). Importantly, the absorber is insensitive to the polarization angle and maintains high solar absorptance within a wide range of incident angles despite its non-symmetrical geometry. Electric field distributions in the TiN metastructure absorber verify that the high absorption can be attributed to the combined effects of the Fabry−Perot interference and localized surface plasmon resonances. The designed photonic device may be promising for solar energy harvesting applications due to its high solar absorptance along with the refractory properties of the materials used. Moreover, the optimization results support that QA-assisted optimization can be useful for designing complex structures such as optical metamaterials.

■ ASSOCIATED CONTENT

Supporting Information

The Supporting Information is available free of charge at https://pubs.acs.org/doi/10.1021/acsami.3c08214.

Design baseline of the metastructure solar absorber, solar spectral irradiance, optimization results, and electric field analysis (PDF)

■ AUTHOR INFORMATION

Corresponding Authors

Guoping Xiong − *University of Texas at Dallas, Richardson, Texas 75080, United States; Department of Mechanical Engineering, University of Texas at Dallas, Richardson, Texas 75080, United States*; Email: Guoping.Xiong@utdallas.edu

Tengfei Luo − *Department of Aerospace and Mechanical Engineering, University of Notre Dame, Notre Dame, Indiana 46556, United States*; orcid.org/0000-0003-3940-8786; Email: tluo@nd.edu

Authors

Seongmin Kim − *Department of Aerospace and Mechanical Engineering, University of Notre Dame, Notre Dame, Indiana 46556, United States*; orcid.org/0000-0001-5906-3004

Shiwen Wu − *University of Texas at Dallas, Richardson, Texas 75080, United States; Department of Mechanical Engineering, University of Texas at Dallas, Richardson, Texas 75080, United States*

Ruda Jian − *University of Texas at Dallas, Richardson, Texas 75080, United States; Department of Mechanical Engineering, University of Texas at Dallas, Richardson, Texas 75080, United States*

Complete contact information is available at: https://pubs.acs.org/10.1021/acsami.3c08214

https://doi.org/10.1021/acsami.3c08214
ACS Appl. Mater. Interfaces 2023, 15, 40606−40613

Author Contributions

S.K. and S.W. contributed equally to this work. S.K., S.W., G.X., and T.L. conceived the research. S.K. and S.W. designed the metastructure absorber. S.K., S.W., and R.J. constructed the absorber model in simulation. S.W. and S.K. analyzed the designed absorber. G.X. and T.L. supervised the overall research. All authors discussed the manuscript.

Funding

T.L. acknowledges the support from the National Science Foundation (grant Nos. 1937923 and 1949910). G.X. acknowledges the support from the University of Texas at Dallas startup fund and the National Science Foundation (grant Nos. 1937949 and 1949962).

Notes

The authors declare no competing financial interest.

REFERENCES

(1) Guldi, D. M.; Rahman, G. M. A.; Prato, M.; Jux, N.; Qin, S.; Ford, W. Single-Wall Carbon Nanotubes as Integrative Building Blocks for Solar-Energy Conversion. *Angew. Chem., Int. Ed.* **2005**, *44*, 2015−2018.

(2) Ge, J.; Yu, Y.; Yan, Y. Earth-Abundant Orthorhombic $BaCu_2Sn(Se_xS_{1-x})_4$ ($x \approx 0.83$) Thin Film for Solar Energy Conversion. *ACS Energy Lett.* **2016**, *1*, 583−588.

(3) Xia, P.; Xu, S.; Wang, C.; Ban, D. Perovskite Luminescent Solar Concentrators for Photovoltaics. *APL Photonics* **2021**, *6*, 120901.

(4) Blackburn, J. L. Semiconducting Single-Walled Carbon Nanotubes in Solar Energy Harvesting. *ACS Energy Lett.* **2017**, *2*, 1598−1613.

(5) Chang, C. C.; Kort-Kamp, W. J. M.; Nogan, J.; Luk, T. S.; Azad, A. K.; Taylor, A. J.; Dalvit, D. A. R.; Sykora, M.; Chen, H. T. High-Temperature Refractory Metasurfaces for Solar Thermophotovoltaic Energy Harvesting. *Nano Lett.* **2018**, *18*, 7665−7673.

(6) Lee, B.; Lentz, R.; Burger, T.; Roy-Layinde, B.; Lim, J.; Zhu, R. M.; Fan, D.; Lenert, A.; Forrest, S. R. Air-Bridge Si Thermophotovoltaic Cell with High Photon Utilization. *ACS Energy Lett.* **2022**, *7*, 2388−2392.

(7) Rephaeli, E.; Fan, S. Absorber and Emitter for Solar Thermophotovoltaic Systems to Achieve Efficiency Exceeding the Shockley-Queisser Limit. *Opt. Express* **2009**, *17*, 15145−15159.

(8) Ungaro, C.; Gray, S. K.; Gupta, M. C. Black Tungsten for Solar Power Generation. *Appl. Phys. Lett.* **2013**, *103*, 071105.

(9) Ungaro, C.; Gray, S. K.; Gupta, M. C. Solar Thermophotovoltaic System using Nanostructures. *Opt. Express* **2015**, *23*, 1149−1156.

(10) Yu, P.; Besteiro, L. V.; Huang, Y.; Wu, J.; Fu, L.; Tan, H. H.; Jagadish, C.; Wiederrecht, G. P.; Govorov, A. O.; Wang, Z. Broadband Metamaterial Absorbers. *Adv. Opt. Mater.* **2018**, *7*, 1800995.

(11) Yang, Z.; Zhang, Y.; Dong, Q.; Lin, J.; Lin, G.; Chen, J. Maximum Power Output and Parametric Choice Criteria of a Thermophotovoltaic Cell Driven by Automobile Exhaust. *Renewable Energy* **2018**, *121*, 28−35.

(12) Wang, Y.; Liu, H.; Zhu, J. Solar Thermophotovoltaics: Progress, Challenges, and Opportunities. *APL Mater.* **2019**, *7*, 080906.

(13) Bhattacharya, S.; John, S. Photonic Crystal Light Trapping: Beyond 30% Conversion Efficiency for Silicon Photovoltaics. *APL Photonics* **2020**, *5*, 020902.

(14) LaPotin, A.; Schulte, K. L.; Steiner, M. A.; Buznitsky, K.; Kelsall, C. C.; Friedman, D. J.; Tervo, E. J.; France, R. M.; Young, M. R.; Rohskopf, A.; et al. Thermophotovoltaic efficiency of 40%. *Nature* **2022**, *604*, 287−291.

(15) Nam, Y.; Yeng, Y. X.; Lenert, A.; Bermel, P.; Celanovic, I.; Soljačić, M.; Wang, E. N. Solar Thermophotovoltaic Energy Conversion Systems with Two-Dimensional Tantalum Photonic Crystal Absorbers and Emitters. *Sol. Energy Mater. Sol. Cells* **2014**, *122*, 287−296.

(16) Jiang, D.; Yang, W. Refractory Material Based Frequency Selective Emitters/Absorbers for High Efficiency and Thermal Stable Thermophotovoltaics. *Sol. Energy Mater. Sol. Cells* **2017**, *163*, 98−104.

(17) Akselrod, G. M.; Huang, J.; Hoang, T. B.; Bowen, P. T.; Su, L.; Smith, D. R.; Mikkelsen, M. H. Large-Area Metasurface Perfect Absorbers from Visible to Near-Infrared. *Adv. Mater.* **2015**, *27*, 8028−8034.

(18) Mehrabi, S.; Rezaei, M. H.; Zarifkar, A. Ultra-Broadband Metamaterial Absorber Based on Cross-Shaped TiN Resonators. *J. Opt. Soc. Am . A* **2020**, *37*, 697−704.

(19) Ghasemzadeh, F.; Rashed, A. R.; Caglayan, H. Phase Singularity Annihilation in Plasmonic Nano-Apertures via Epsilon-Near-Zero Metamaterials. *APL Photonics* **2021**, *6*, 016101.

(20) Dao, V. D.; Choi, H. S. Carbon-Based Sunlight Absorbers in Solar-Driven Steam Generation Devices. *Glob. Chall.* **2018**, *2*, 1700094.

(21) Zhou, S.; Zhou, G.; Jiang, S.; Fan, P.; Hou, H. Flexible and Refractory Tantalum Carbide-Carbon Electrospun Nanofibers with High Modulus and Electric Conductivity. *Mater. Lett.* **2017**, *200*, 97−100.

(22) Zang, X.; Tai, K. Y.; Jian, C.; Shou, W.; Matusik, W.; Ferralis, N.; Grossman, J. C. Laser-Induced Tar-Mediated Sintering of Metals and Refractory Carbides in Air. *ACS Nano* **2020**, *14*, 10413−10420.

(23) Swearer, D. F.; Knowles, N. R.; Everitt, H. O.; Halas, N. J. Light-Driven Chemical Looping for Ammonia Synthesis. *ACS Energy Lett.* **2019**, *4*, 1505−1512.

(24) Nguyen, N. T.; Yan, T.; Wang, L.; Loh, J. Y. Y.; Duchesne, P. N.; Mao, C.; Li, P. C.; Ali, F. M.; Xia, M.; Ghoussoub, M.; et al. Plasmonic Titanium Nitride Facilitates Indium Oxide CO(2) Photocatalysis. *Small* **2020**, *16*, 2005754.

(25) Li, W.; Guler, U.; Kinsey, N.; Naik, G. V.; Boltasseva, A.; Guan, J.; Shalaev, V. M.; Kildishev, A. V. Refractory Plasmonics with Titanium Nitride: Broadband Metamaterial Absorber. *Adv. Mater.* **2014**, *26*, 7959−7965.

(26) Wu, S.; Luo, T.; Xiong, G. Plasmon Hybridization-Induced Ultra-broadband High Absorption from 0.4 to 1.8 Microns in Titanium Nitride Metastructures. *Plasmonics* **2021**, *16*, 799−809.

(27) Wu, S.; Wu, T.-N.; Xiong, G. Ultra-Broadband High Solar Absorption in Checkerboard-Shaped Titanium Nitride Plasmonic Metastructures. *Opt. Mater.* **2021**, *116*, 111117.

(28) Wang, H.; Chen, Q.; Wen, L.; Song, S.; Hu, X.; Xu, G. Titanium-Nitride-Based Integrated Plasmonic Absorber/Emitter for Solar Thermophotovoltaic Application. *Photonics Res.* **2015**, *3*, 329−334.

(29) Ma, W.; Cheng, F.; Liu, Y. Deep-Learning-Enabled On-Demand Design of Chiral Metamaterials. *ACS Nano* **2018**, *12*, 6326−6334.

(30) Liu, Z.; Zhu, D.; Rodrigues, S. P.; Lee, K. T.; Cai, W. Generative Model for the Inverse Design of Metasurfaces. *Nano Lett.* **2018**, *18*, 6570−6576.

(31) Zhang, T.; Kee, C. Y.; Ang, Y. S.; Ang, L. K. Deep Learning-Based Design of Broadband GHz Complex and Random Metasurfaces. *APL Photonics* **2021**, *6*, 106101.

(32) Finegan, D. P.; Squires, I.; Dahari, A.; Kench, S.; Jungjohann, K. L.; Cooper, S. J. Machine-Learning-Driven Advanced Characterization of Battery Electrodes. *ACS Energy Lett.* **2022**, *7*, 4368−4378.

(33) Kudyshev, Z. A.; Kildishev, A. V.; Shalaev, V. M.; Boltasseva, A. Machine-Learning-Assisted Metasurface Design for High-Efficiency Thermal Emitter Optimization. *Appl. Phys. Rev.* **2020**, *7*, 021407.

(34) Ma, W.; Liu, Z.; Kudyshev, Z. A.; Boltasseva, A.; Cai, W.; Liu, Y. Deep Learning for the Design of Photonic Structures. *Nat. Photonics* **2020**, *15*, 77−90.

(35) Kitai, K.; Guo, J.; Ju, S.; Tanaka, S.; Tsuda, K.; Shiomi, J.; Tamura, R. Designing Metamaterials with Quantum Annealing and Factorization Machines. *Phys. Rev. Res.* **2020**, *2*, 013319.

(36) Wilson, B. A.; Kudyshev, Z. A.; Kildishev, A. V.; Kais, S.; Shalaev, V. M.; Boltasseva, A. Machine Learning Framework for Quantum Sampling of Highly Constrained, Continuous Optimization Problems. *Appl. Phys. Rev.* **2021**, *8*, 041418.

https://doi.org/10.1021/acsami.3c08214
ACS Appl. Mater. Interfaces 2023, 15, 40606−40613

(37) Kim, S.; Shang, W.; Moon, S.; Pastega, T.; Lee, E.; Luo, T. High-Performance Transparent Radiative Cooler Designed by Quantum Computing. *ACS Energy Lett.* **2022**, *7*, 4134−4141.
(38) Palik, E. D. *Handbook of Optical Constants of Solids*; Academic Press, 1998; Vol. 3.
(39) Mehrabi, S.; Rezaei, M. H.; Rastegari, M. R. High-Efficient Plasmonic Solar Absorber and Thermal Emitter from Ultraviolet to Near-Infrared Region. *Opt. Laser Technol.* **2021**, *143*, 107323.
(40) Wan, W.; Luo, M.; Su, Y. Ultrathin Polarization-Insensitive, Broadband Visible Absorber Based Rectangular Metagratings. *Opt. Commun.* **2020**, *458*, 124857.
(41) Kang, Y.; Wang, J.; Liu, H. A Dual-Band Polarization Insensitive Metamaterial Absorber with a Single Square Metallic Patch for Sensing Application. *Plasmonics* **2021**, *17*, 449−456.
(42) Qin, F.; Chen, X.; Yi, Z.; Yao, W.; Yang, H.; Tang, Y.; Yi, Y.; Li, H.; Yi, Y. Ultra-Broadband and Wide-Angle Perfect Solar Absorber Based on TiN Nanodisk and Ti Thin Film Structure. *Sol. Energy Mater. Sol. Cells* **2020**, *211*, 110535.
(43) Mehrabi, S.; Bilal, R. M. H.; Naveed, M. A.; Ali, M. M. Ultra-Broadband Nanostructured Metamaterial Absorber Based on Stacked Square-Layers of TiN/TiO2. *Opt. Mater. Express* **2022**, *12*, 2199−2211.
(44) Liu, Z.; Aydin, K. Localized Surface Plasmons in Nanostructured Monolayer Black Phosphorus. *Nano Lett.* **2016**, *16*, 3457−3462.
(45) Awang, R. A.; El-Gohary, S. H.; Kim, N.-H.; Byun, K. M. Enhancement of Field−Analyte Interaction at Metallic Nanogap Arrays for Sensitive Localized Surface Plasmon Resonance Detection. *Appl. Opt.* **2012**, *51*, 7437−7442.
(46) Liu, N.; Guo, H.; Fu, L.; Kaiser, S.; Schweizer, H.; Giessen, H. Plasmon Hybridization in Stacked Cut-Wire Metamaterials. *Adv. Mater.* **2007**, *19*, 3628−3632.
(47) Gonçalves, P. A. D.; Xiao, S.; Peres, N. M. R.; Mortensen, N. A. Hybridized Plasmons in 2D Nanoslits: From Graphene to Anisotropic 2D Materials. *ACS Photonics* **2017**, *4*, 3045−3054.
(48) Wen, X.; Li, G.; Gu, C.; Zhao, J.; Wang, S.; Jiang, C.; Palomba, S.; Martijn de Sterke, C.; Xiong, Q. Doubly Enhanced Second Harmonic Generation through Structural and Epsilon-near-Zero Resonances in TiN Nanostructures. *ACS Photonics* **2018**, *5*, 2087−2093.
(49) Guo, H.; Chen, W.; Shan, Y.; Wang, W.; Zhang, Z.; Jia, J. Microstructures and Properties of Titanium Nitride Films Prepared by Pulsed Laser Deposition at Different Substrate Temperatures. *Appl. Surf. Sci.* **2015**, *357*, 473−478.
(50) Ouellette, O.; Hossain, N.; Sutherland, B. R.; Kiani, A.; García de Arquer, F. P.; Tan, H.; Chaker, M.; Hoogland, S.; Sargent, E. H. Optical Resonance Engineering for Infrared Colloidal Quantum Dot Photovoltaics. *ACS Energy Lett.* **2016**, *1*, 852−857.
(51) Zhu, W.; Zheng, G.; Cao, S.; He, H. Thermal Conductivity of Amorphous SiO_2 Thin Film: A Molecular Dynamics Study. *Sci. Rep.* **2018**, *8*, 10537.

https://doi.org/10.1021/acsami.3c08214
ACS Appl. Mater. Interfaces 2023, 15, 40606−40613